
**ELECTRONIC PROPERTIES
OF SOLID**

The Andreev Conductance in Superconductor–Insulator–Normal Metal Structures

A. V. Seliverstov^{a,b,d}, M. A. Tarasov^c, and V. S. Edel'man^{a*}

^a Kapitza Institute for Physical Problems, Russian Academy of Sciences, Moscow, 119334 Russia

^b Moscow Institute of Physics and Technology (State University), Dolgoprudnyi, Moscow oblast, 141701 Russia

^c Kotel'nikov Institute of Radio Engineering and Electronics, Russian Academy of Sciences, Moscow, 125009 Russia

^d Laboratory of Solid-State Physics and Magnetism, KU Leuven, BE-30001, Belgium

*e-mail: vsedelman@yandex.ru

Received October 7, 2016

Abstract—The Andreev subgap conductance at 0.08–0.2 K in thin-film superconductor (aluminum)—insulator—normal metal (copper, hafnium, or aluminum with iron-sublayer-suppressed superconductivity) structures is studied. The measurements are performed in a magnetic field oriented either along the normal or in the plane of the structure. The dc current–voltage (I – U) characteristics of samples are described using a sum of the Andreev subgap current dominating in the absence of the field at bias voltages $U < (0.2–0.4)\Delta_c/e$ (where Δ_c is the energy gap of the superconductor) and the single-carrier tunneling current that predominates at large voltages. To within the measurement accuracy of 1–2%, the Andreev current corresponds to the formula $I_n + I_s = K_n \tanh(eU/2kT_{\text{eff}}) + K_s(eU/\Delta_c)/\sqrt{1 - eU/\Delta_c}$ following from a theory that takes into account mesoscopic phenomena with properly selected effective temperature T_{eff} and the temperature- and field-independent parameters K_n and K_s (characterizing the diffusion of electrons in the normal metal and superconductor, respectively). The experimental value of K_n agrees in order of magnitude with the theoretical prediction, while K_s is several dozen times larger than the theoretical value. The values of T_{eff} in the absence of the field for the structures with copper and hafnium are close to the sample temperature, while the value for aluminum with an iron sublayer is several times greater than this temperature. For the structure with copper at $T = 0.08–0.1$ K in the magnetic field $B_{\parallel} = 200–300$ G oriented in the plane of the sample, the effective temperature T_{eff} increases to 0.4 K, while that in the perpendicular (normal) field $B_{\perp} \approx 30$ G increases to 0.17 K. In large fields, the Andreev conductance cannot be reliably recognized against the background of single-carrier tunneling current. In the structures with hafnium and in those with aluminum on an iron sublayer, the influence of the magnetic field is not observed.

DOI: 10.1134/S1063776117030153

1. INTRODUCTION

Conductance in superconductor–insulator–normal metal (SIN) type structures has been extensively studied. This interest is related to prospects of using these structures in low-temperature thermometers [1, 2], electronic cooling devices [1, 3], and high-sensitivity bolometers [4]. The main mechanism of tunneling current transfer and accompanying processes—heating and electron cooling—in these structures is commonly believed to be the single-particle tunneling of electrons (holes) from the normal metal to superconductor, to its free states above (below) the energy gap Δ_c .

The phenomenon of Andreev reflection that determines the conductance of SN contacts is usually not observed in tunnel structures against the background of single-particle tunneling. In the case of large electron mean free paths, the probability of tunneling with

Andreev reflection, being a two-particle process, is small [5]. However, at temperatures $T \ll T_c = \Delta_c/1.76k$ (T_c is the superconducting transition temperature and k is the Boltzmann constant) and small voltages on the tunnel junction ($U \ll V_{\Delta} = \Delta_c/e$), the normal electron current exponentially decays and the Andreev current may become dominating as has been observed in some experiments [6–11]. The relative increase in this current is favored by the fact that, in real planar SIN structures with small thickness of the normal electrode and short free-path times τ_{el} for elastic collisions, the electron–hole Andreev pair exhibits multiple “falls” on the interface during dephasing caused by inelastic collisions with characteristic time $\tau_{\text{p}} \gg \tau_{\text{el}}$, thus proportionally increasing the probability of tunneling (see, e.g., [12], where it has been shown that the Andreev subgap current I_{subgap} consists of two compo-

nents, I_n and I_s , related to the diffusion motion of electrons in the normal and superconducting electrodes, respectively). In the case of tunnel junctions with dimensions exceeding lengths $\sqrt{\hbar D/\max(eU, kT)}$, $\sqrt{\hbar D/\Delta_c}$ (D is the diffusion length) or the mean free path with dephasing (l_ϕ), the Andreev current obeys the following relation [12]:

$$I_{\text{subgap}}(U, T) = I_n + I_s = \frac{\hbar}{e^3 R_n^2 S v_n d_n} \tanh\left(\frac{eU}{2kT}\right) + \frac{\hbar}{e^3 R_n^2 S v_s d_s 2\pi \sqrt{1 - eU/\Delta_c}}, \quad (1)$$

where v_n and v_s are the densities of electron states in the normal and superconducting electrodes, respectively; d_n , d_s , and S are the corresponding thicknesses and the SN contact area; R_n is the junction resistance in the normal state; and U is the voltage on the tunnel junction.

The existence of Andreev conductance is, in principle, established. However, there are several questions that still have to be experimentally elucidated, and the present work is devoted to these issues as formulated below.

(i) According to some works [6–10], the current–voltage (I – U) characteristics measured for small-size junctions are in satisfactory agreement with the theory [12] for SIN structures with strongly different areas S of tunnel junctions (from $0.018 \mu\text{m}^2$ [10] and $0.023 \mu\text{m}^2$ [6] to $0.45 \mu\text{m}^2$ [8]) and transparencies of the tunnel junction characterized by the product $R_n S$ (from $30 \Omega \mu\text{m}^2$ [6] to $390 \Omega \mu\text{m}^2$ [7, 8] and within 26 – $3500 \Omega \mu\text{m}^2$ [10]). Lowell et al. [9] established that, for tunnel junctions with $S = 4$ – $16 \mu\text{m}^2$ and $R_n S = 30$ – $200 \Omega \mu\text{m}^2$, the theory and experiment are consistent to within 10–20%. The presence of the I_s component was not discussed, but according to data reported in [9], it can be concluded that its contribution amounts to 10–20% of I_n . In our recent work [11] (for SIN junctions with $S = 8$ – $10 \mu\text{m}^2$ and $R_n S = 560 \Omega \mu\text{m}^2$), it was pointed out that, for I_n values close to theoretical, the I_s component was comparable with I_n and several dozen times larger than that predicted by formula (1). However, taking into account that d_s of superconducting electrodes in samples studied in [9] was 3–6 times larger than that in [11] and that I_s according to formula (1) is proportional to $1/d_s$, these data do not contradict each other. Nevertheless, the question of I_s contribution to the total current has to be given attention.

(ii) It would be of interest to study the temperature dependence of conductance $G_{\text{subgap}} = G_n + G_s$. Relation (1) shows that, at low voltages on the junction, $G_n \approx 1/T$ and G_s is temperature independent. According to [13], G_n should tend to be constant at low temperatures owing to the electron–electron interaction. To the best of our knowledge, the temperature depen-

dence of the Andreev conductance was experimentally studied in only one work [6], where it was established that $G_{\text{subgap}} \approx 1/T$ in a temperature interval of 27–220 mK at low bias voltages. Therefore, this issue has not yet been studied in sufficient detail.

(iii) From general considerations, it could be expected that the Andreev current must depend on the magnetic field. Indeed, the study [6] of an interferometer comprising a superconducting circuit closed by a short strip of normal metal forming a SINIS junction revealed the current variations (similar to those in a SQUID) caused by changes in magnetic field B_\perp perpendicular to the plane of structure. These variations are related to changes in the phase of the wave function in a doubly connected superconductor, but do not depend on the dephasing of electron–hole pairs in the volume of a single SIN junction. It was established [10, 11] that the Andreev conductance was suppressed in the magnetic field B_\parallel parallel to the tunnel junction plane. Previously, we studied [14] the behavior of flat SINIS structures in magnetic field B_\perp perpendicular to the structure plane and established that the superconducting junction in this configuration features an Abrikosov system of quantum vortices with normal cores that leads to increase in the single-particle conductance. However, no pronounced subgap conductance was observed in the samples used in [14] and the influence of the perpendicular magnetic field on this component remained unknown.

(iv) In all the known experiments where the Andreev conductance was observed in SIN structures, the samples were prepared from same materials: aluminum as a superconductor and copper as a normal metal. In addition to this combination, we also studied the junctions comprising aluminum–aluminum with iron sublayer suppressing superconductivity and aluminum–hafnium.

2. INVESTIGATION OF ALUMINUM–ALUMINUM OXIDE–COPPER STRUCTURES

Most of these investigations were performed with sample S55 comprising four identical SIN junctions arranged on a silicon chip (Fig. 1). Two junctions (1 and 4) were situated at the ends of a 30-nm-thick copper strip, and the other two junctions (2 and 3) were situated in the middle of this strip. Copper was deposited onto the oxidized surface of a 80-nm-thick aluminum layer (with oxide thickness about 1 nm). Aluminum was first deposited onto gold-based electrodes and then etched to obtain windows 5–7. As a result, three suspension copper bridges were formed in each structure. The technology is described in more detail elsewhere [15]. The structures had somewhat different areas S , of tunnel junctions (8 or $10 \mu\text{m}^2$) and lengths L_n of suspended normal-metal strips (2 or $4 \mu\text{m}$).

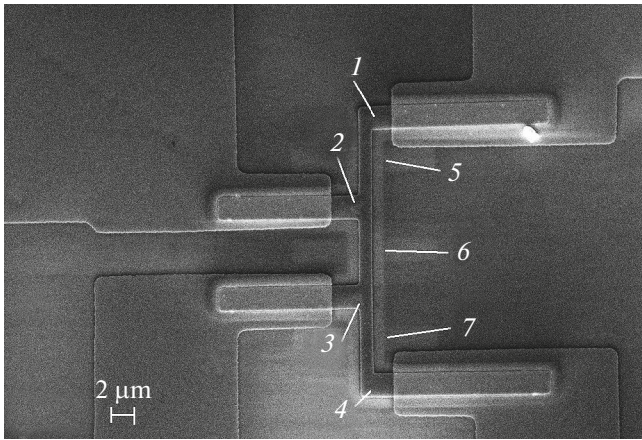


Fig. 1. Electron-microscopic image of the multielement SINIS structure on a silicon chip: (1–4) SIN tunnel junctions; (5–7) copper suspension bridges.

An important parameter of SIN structures was the coefficient of electron diffusion in metal films. For a copper film, this parameter could be estimated by measuring the resistance of a 4- μm bridge between junctions 2 and 3 for the current transferred via junctions 1 and 4. This value was about 6 Ω , which yielded the resistivity of copper film of about 5 $\mu\Omega\text{cm}$ and corresponded to the electron mean free path $l_e \approx 10\text{ nm}$ or the electron diffusion coefficient $D \approx 70\text{ cm}^2/\text{s}$. For aluminum film, the correlation length was estimated as [14]

$$\xi \approx \sqrt{\xi_0 l_e} \approx 100\text{ nm},$$

where $\xi_0 \approx 1.5\text{ }\mu\text{m}$ is the value for pure bulk aluminum. Then, the electron mean free path in aluminum is $l_e \approx 8\text{ nm}$.

The dc current–voltage (I – U) characteristics were measured using the conventional four-point-probe scheme. The tunnel junctions were protected against parasitic radiation from connecting paths by 0.8-M Ω resistors cooled to 0.4 K. The sample structure topology allowed studying the characteristics of SINIS junctions (e.g., by passing current via junctions 1 and 4 and measuring the corresponding voltage drops) and single SIN junctions (e.g., by passing current via junctions 1 and 4 and measuring the voltage on contacts 1 and 2).

The data acquisition system was based on a notebook computer with NI ESB unit. The probing current I was set by a 16-bit digital-to-analog converter. The bias voltage U was amplified by a low-noise pre-amplifier and processed by a 16-bit analog-to-digital converter. The differential conductance $G(U) = dI/dU$ and differential resistance R_d were determined by numerical integration of I – U characteristics.

The measurements were performed with the aid of a dilution cryostat insert [16], in which the samples were mounted on top of the device inside a screen

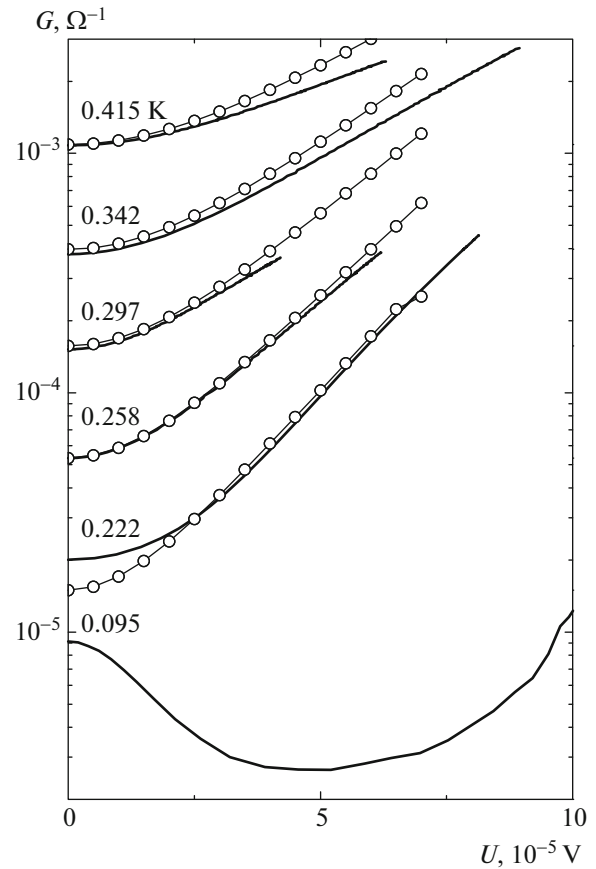


Fig. 2. Curves of measured conductance $G(U)$ in comparison to values (circles) calculated by formula (2) with $\Delta_c/k = 2.2\text{ K}$ and $R_n = 27\text{ }\Omega$ at various temperatures (indicated at the curves) for SIN junction 2 in the structure imaged in Fig. 1.

maintaining temperature within 0.4–0.5 K, in a holder cooled below 0.1 K. The samples could be moved in both horizontal and vertical directions. A vertically oriented magnetic field was created by a coil mounted outside the cryostat and could be applied to a sample in approximately the normal direction or in the plane of the tunnel junction. The field orientation could be varied by tilting the coil within $\pm 10^\circ$.

All junctions exhibited generally similar I – U curves and, hence, similar $G(U, T)$ dependences (Fig. 2). At 0.25 K $< T < 0.45$ K, these curves were well described by the derivative of the well-known expression for single-particle tunneling [2, 17]:

$$I(U, T) = \frac{1}{eR_n} \sqrt{2\pi k T \Delta_c} \exp\left(-\frac{\Delta_c}{kT}\right) \sinh\left(\frac{eU}{kT}\right). \quad (2)$$

As can be seen from this equation, gap Δ_c determines the relative values of $G(U=0, T)$ and R_n sets the absolute scale of current. Since the G value exhibits more than tenfold variation in the indicated temperature interval, it is possible to determine Δ_c and R_n to within 5 and 10%, respectively, from experimental data.

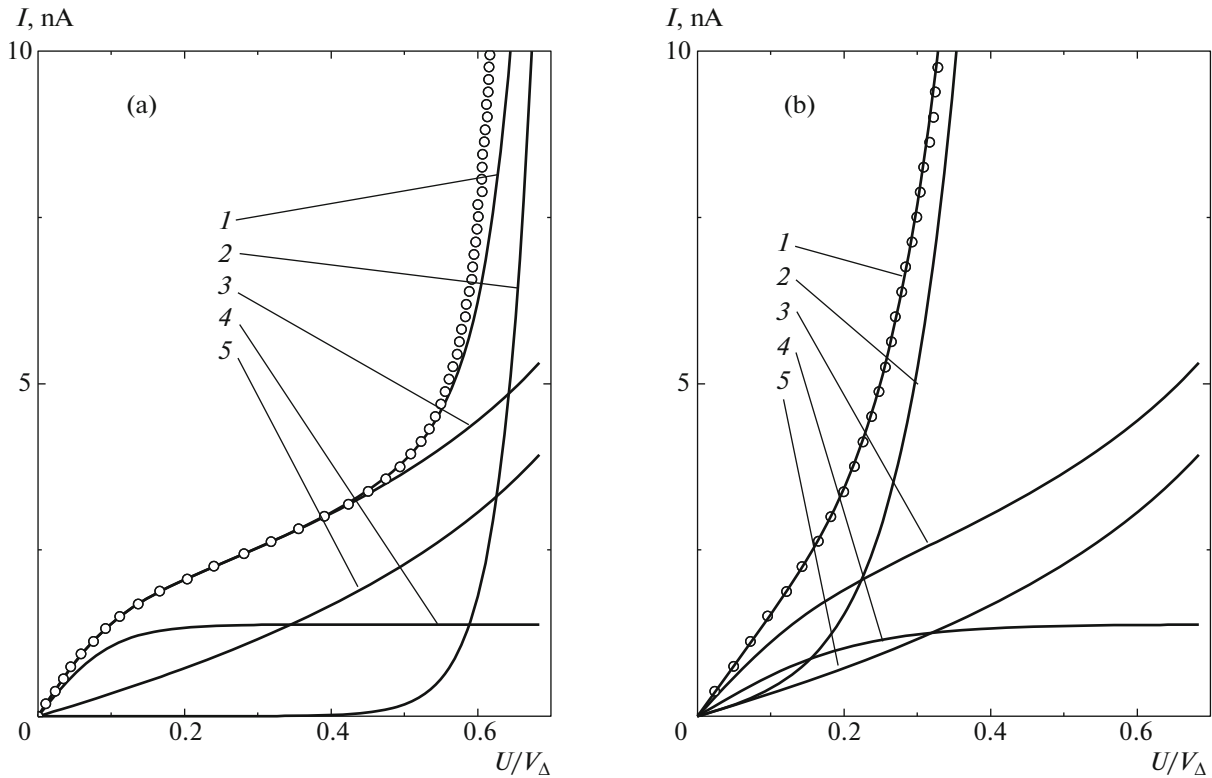


Fig. 3. Measured $I-U$ characteristics (circles) of SIN junction 2 (Fig. 1) at (a) $T = 0.095$ K and (b) $T = 0.18$ K in comparison to the results of calculations (curves): (1) total current; (2) single-particle current according to formula (2) for same temperatures and parameters indicated in the legend to Fig. 2; (3) total Andreev current including components (4) I_n and (5) I_s according to formula (3) with $K_n = 0.138$ nA and $K_s = 0.33$ nA and (a) $T_{\text{eff}} = 0.11$ K and (b) $T_{\text{eff}} = 0.18$ K.

Direct measurement of R_n in the system under consideration was impossible because the resistance of current-carrying paths connecting tunnel junctions to contact pads on the silicon chip was comparable with or even greater than R_n . As can be seen from Fig. 2, the results of calculations agree with measured values at temperatures above 0.25 K and small voltages, while at $U > 40$ μ V the measured conductance becomes somewhat smaller than calculated. This is probably related to electronic cooling, which is most effective in this temperature range [1, 3].

When the temperature decreases, a shunting component to the conductance appears that is due to the Andreev current and weakly depends on the temperature. For this reason, the total conductance at $T = 0.222$ K is about one and a half times greater than the single-particle conductance (see Fig. 2) and significantly exceeds it at about 0.1 K; at $U = 0$, the $G(T)$ curve exhibits a maximum.

The $G(T)$ maximum was observed for all SIN and SINIS structures studied, but the $G(0)$ value not only varied from one structure to another, but also changed for the same structure upon keeping it at room temperature. This was apparently related to some uncontrolled processes during sample manufacturing and to

diffusion and corrosion phenomena taking place during storage (see the table below). At temperatures below 0.2 K, the Andreev current is comparable to that of single-particle tunneling; on attaining about 0.1 K, the Andreev current significantly exceeds the single-particle current (see Figs. 2 and 3).

In calculations of the single-particle current by Eq. (2), the junction temperature was refined by coincidence with experiment in the initial region, where heating caused by the probing current was at a minimum. As can be seen from Fig. 3a, this heating was actually significant because of poor heat exchange at low temperatures, leading to more rapid growth in the current with increasing voltage. However, the temperature correction in the initial region did not exceed several millikelvin in comparison to readings of the RuO₂-based resistance thermometer.

The description of results concerning the Andreev current was based on relation (1), which was derived [12] for the case where the tunnel junction size was greater than $\sqrt{\hbar D / \max(eU, kT)}$, $\sqrt{\hbar D / \Delta_c}$ or the mean free path with dephasing ($l_\phi \approx 1.5$ according to measurements [18] with a correction for the diffusion length D in our samples). These conditions were satisfied in the case under consideration. Formula (1) takes

into consideration the two currents that appear owing to the interference of pairs in the bulk of normal metal (I_n) and in the bulk of superconductor (I_s).

In order to compare the dependence of type (1) to experiment, we selected three parameters—coefficients K_n and K_s and effective temperature T_{eff} —in formula (1) rewritten as

$$I_n + I_s = K_n \tanh\left(\frac{eU}{2kT_{\text{eff}}}\right) + K_s \frac{eU/\Delta_c}{\sqrt{1 - eU/\Delta_c}}. \quad (3)$$

The values of K_n , K_s , and T_{eff} were selected to provide an error within 3–5% at $T \approx 0.08$ –0.1 K. It was found that, in this temperature interval, the agreement with experiment could be achieved without changing K_n and K_s by only varying the value of T_{eff} . However, the error of determining this parameter somewhat increased because of the uncertainty of determining the shunting single-particle current, reaching 10% at $T = 0.18$ K. Figure 4 shows plots of T_{eff} for two adjacent SIN junctions 1 and 2 in the structure studied (see Fig. 1). As can be seen, T_{eff} somewhat exceeds the sample temperature at $T < 0.1$ K; the two temperatures become equal at $T > 0.15$ K, in agreement with theoretical formula (1). The deviation from this formula at low temperatures is probably related to the electron–electron interaction as has been pointed in [13].

Results for several SIN and SINIS junctions in five structures with the same topology shown in Fig. 1 are presented in the table. Three structures (S55_1–S55_3) were arranged on the same silicon wafer, S33 was analogous to S55_1, and S9 had a more transparent insulating layer. These data were obtained at $T \approx 0.08$ –0.1 K, where the I – U curves at low voltages were independent of the temperature to within the error of measurements. In calculations of parameters for SINIS structures, the junctions of each pair were assumed to be identical (although data in the table reveal some differences). Values in the table refer to one junction and were obtained by substituting the voltage divided by 2 into formula (3). In all cases, Eq. (3) provided the fitting to experiment within 1–2%. However, this could only be achieved at the expense of significant variation of the parameters. The values of effective temperature were rather close, but in all cases, they somewhat exceeded the temperature of junctions measured by the resistance thermometer and refined with respect to single-particle conductance.

The values of K_n and K_s for various nominally identical junctions show two- to threefold differences. In addition, the parameters of junctions exhibited temporal variation: for SINIS junction 1, 4 (S55_1 structure, lines 1 and 2 in the table), the parameters characterizing the Andreev current and the values of Δ_c and R_n changed after storage for 10 days at room temperature. For other junctions, the temporal changes were slower (see lines 3–8 in the table). From these data, it

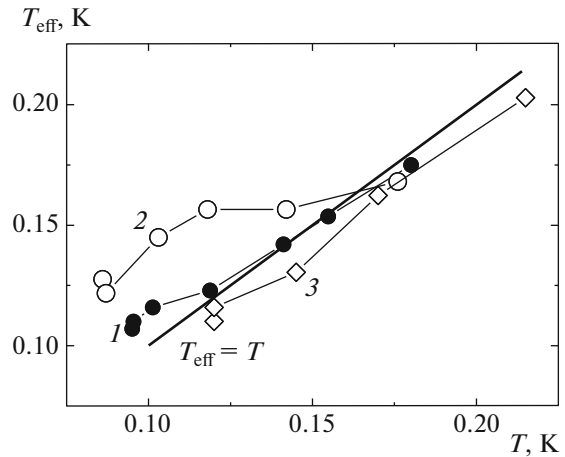


Fig. 4. Plots of effective temperature T_{eff} in formula (3) vs. sample temperature determined from single-particle current for SIN junction 1 (open circles), SIN junction 2 (black circles), and SINIS junction (3) aluminum–aluminum oxide–hafnium (rhombs). Error at $T \leq 0.15$ K corresponds to sizes of symbols; error at $T = 0.18$ –0.22 K is on the order of 10%; error of temperature determination is about 5% (1, 2) and about 10% (3).

might be concluded that diffusion, annealing, and corrosion processes involved all layers in the structures studied. The values of coefficient K_n presented in the table were calculated according to formula (1), where the densities of electron states ν_n and ν_s were assumed to be $1.56 \times 10^{47} \text{ J}^{-1} \text{ m}^{-3}$ for copper [19] and $3.02 \times 10^{47} \text{ J}^{-1} \text{ m}^{-3}$ for aluminum [20], as follows from the electronic heat capacities of these metals. As can be seen, these theoretical estimates significantly differ from the measured values. It should be noted that differences on the same order of magnitude were reported in [6, 7, 10].

Formulas (1) and (3) yield the following relation:

$$K_s/K_n = \nu_n d_n / 2\pi \nu_s d_s = 0.03.$$

As can be seen from data in the table, the experimental ratio is two orders of magnitude greater than the theoretical value and varies from 2.5 to 7.5 on the passage from one junction to another. This circumstance was previously pointed out in [11].

It is difficult to explain this large discrepancy between theory and experiment. Apparently, the theory does not take into account all significant factors. In particular, the boundary between layers is far from being flat, as is evident from [14, Fig. 1]. Therefore, the insulating layer can hardly be constant and the probability of tunneling cannot be adequately described by its average value determined by R_n .

The subgap conductance in SIN structures can also be considered in the framework of another approach, where an additional current is introduced as related to smearing of the excitation spectrum and

Data for several SIN and SINIS junctions in five structures with the same topology shown in Fig. 1

No.	Structure	Junctions/ S , μm^2	T_{eff} , K ($T < 0.1$ K)	K_n , nA	K_n , nA formula (1)	K_s , nA	K_s/K_n	Δ_c , K	R_n , Ω	Date
1	S55_1	1, 4/8	0.143	0.07	0.19	0.23	3.3	2.20	55	19.10.2015
2	1	1, 4	0.143	0.045	0.086	0.265	5.9	1.98	80	29.10.2015
3	1	2, 3/10	0.122	0.034	—	0.25	7.4	—	—	19.10.2015
4	1	2, 3	0.14	0.04	—	0.22	5.5	—	—	04.11.2015
5	2	1, 4/8	0.122	0.12	—	0.38	3.2	—	—	19.10.2015
6	2	1, 4	0.155	0.095	—	0.39	4.1	—	—	25.11.2015
7	2	1	0.162	0.13	0.40	0.39	3.0	2.02	37	25.11.2015
8	2	1	0.116	0.07	0.34	0.39	5.6	2.05	40	17.06.2016
9	2	4	0.127	0.112	0.15	0.25	2.2	1.93	60	25.11.2015
10	2	2, 3/10	0.108	0.13	—	0.62	4.8	—	—	19.10.2015
11	2	2	0.107	0.135	0.75	0.32	2.4	2.2	27	17.06.2016
12	3	1, 4/8	0.130	0.07	—	0.35	5.0	—	—	19.10.2015
13	3	1, 4	0.145	0.06	—	0.35	5.8	—	—	05.11.2015
14	S33	1, 4	0.116	0.08	—	0.27	3.4	—	—	19.10.2015
15	S9	3/10	0.116	8.0	—	39	4.9	2.1	10	10.07.2016
16	Al–Hf	SINIS/8	0.110	0.24	0.0015	0.09	0.37	1.9	480	21.12.2015
17	Al–Hf	SINIS/8	0.120	0.19	—	0.26	1.35	—	—	15.03.2016
18	Al–Al(Fe)	100 SIN/2	0.56	0.043	—	0.11	2.5	1.98	115	20.02.2015

described by the Dynes fitting parameter γ , i.e., by replacing Δ_c with $\Delta_c(1 + i\gamma)$. The expression for this additional current is as follows [2]:

$$I_{\text{Dy}} = \frac{\gamma U / R_n}{\sqrt{1 - (eU / \Delta_c)^2}}. \quad (4)$$

This formula is qualitatively different from expression (3) for I_s , since a square (rather than first power) of voltage U is under the root sign. The result can be seen in Fig. 5, where the experimental I – U curve after subtraction of the Andreev current corresponding to formula (3) coincides (to within the noise) with the calculated single-particle current. In the case of formula (4) with $\gamma/R_n = 1.5 \times 10^{-6}$ and $\gamma = 10^{-4}$, the current significantly exceeds noises in the interval of $U/V_\Delta = 0.25$ – 0.5 . On the basis of this result, we believe that it would be correct to describe the Andreev subgap current using formula (3).

Measurements in Magnetic Field

The first investigations of the Andreev conductance in SINIS and SIN structures exposed to the tangent magnetic field B_{\parallel} parallel to the sample plane were undertaken in [10, 11]. Recently, we performed

measurements [14] in the magnetic field B_{\perp} perpendicular to the sample surface, but the Andreev conductance in these samples was not as clearly manifested as before [11]. Therefore, it was of interest to perform such measurements on the same sample. In the present work, the magnetic field was created by a coil mounted outside the cryostat and was oriented in the vertical direction. Therefore, after measuring sample S55 in one (vertical) position, it was necessary to warm it up to room temperature and rapidly mount it in a different (horizontal) position so as to avoid changes in parameters of the structure. In fact, this rearrangement was performed within one day. Measurements showed that characteristics of the sample were retained to within the error of measurements.

During the work with S55 sample for a long period of time, the most pronounced Andreev conductance was retained in only one SIN junction, the parameters of which are presented in the table (line 11). Figure 6 shows the plots of conductance G versus voltage for various values of the magnetic field applied in the plane (Fig. 6a) or in the normal direction (Fig. 6b). Similar to experiments described in [11], the field direction in the plane of the structure was adjusted so

as to minimize its influence on the single-particle tunneling conductance dominating at $U/V_\Delta > 0.3$.

For the in-plane magnetic field B_\parallel , the conductance $G(U = 0, B_\parallel)$ related to the Andreev current begins to decrease, while the conductance at $U/V_\Delta > 0.3$ (related to the single-particle tunneling) grows (Fig. 6a). A change in the contribution due to single-particle tunneling with increasing B_\parallel can be related to an error of adjustment and/or edge effects leading to normal regions in the junction. As for the Andreev tunneling, the conductance caused by this phenomenon drops to one-third with increasing B_\parallel (at a maximum possible field of 280 G).

An analogous picture of decrease in the conductance at $U = 0$ was also observed in the normal field B_\perp . However, the Andreev conductance in this case is clearly manifested up to a field of about 30 G. In stronger fields, this conductance overlaps with the single-particle component (Fig. 6b).

For a quantitative characterization of changes in the subgap current under the action of a magnetic field, we used formula (3). Similar to the case of experiments with variable temperature, it was found that, in the entire range of magnetic field variation for both orientations, the agreement of calculations and experiment to within 1–2% could be achieved by changing the T_{eff} value alone (Fig. 7). Figure 8 shows the corresponding plot of $T_{\text{eff}}(B)$. As can be seen, characteristic fields corresponding to the rapid variation of T_{eff} are within 100–200 G for B_\parallel and about 30 G for B_\perp .

Characteristic values of magnetic induction (1–2 kG) corresponding to the rapid variation of conductance observed in [10] were about an order of magnitude greater than those in our experiments (according to formula (3), the field-dependent conductance component G_n is proportional to $1/T_{\text{eff}}$). This result agrees with the fact that the size of tunnel junctions in [10] was about tenfold smaller.

The effect of magnetic field on the Andreev conductance in SININ structures was studied in [21, 22]. It was pointed out that, since a field-dependent phase $2\pi\lambda y B/\Phi_0$ in the transverse direction y appeared in the superconductor under the action of in-plane field B_\parallel , the Andreev current was suppressed by the field proportional to the phase shift on path length $y \approx \xi_n$. Here, λ is the field penetration depth (in pure aluminum, $\lambda = 30$ nm), ξ_n is the correlation length in the normal metal (in our structure, $\xi_n \approx 10$ –20 nm), and Φ_0 is the magnetic flux quantum. These values correspond to a characteristic field of $B \approx 5$ –10 G.

According to our recent results [14], in-plane field B_\parallel in the case under consideration is almost homogeneous in the volume of the tunnel junction, since the depth of field penetration into the superconducting film is $\lambda > 300$ nm. It can be expected that magnetic

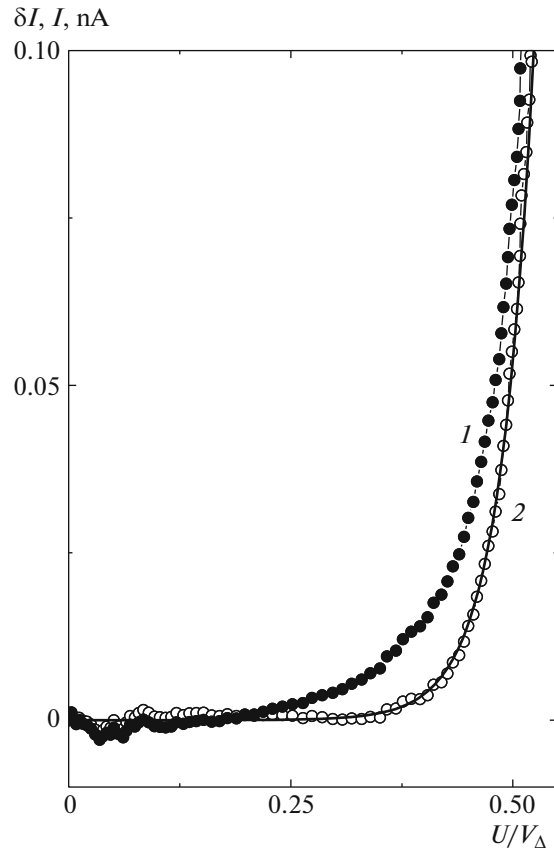


Fig. 5. I – U curves of SIN junction with subtracted (1) Andreev current calculated by formula (3) and I_{Dy} calculated by formula (4); (2) $I_n + I_s$, formula (3); solid curve shows single-particle current according to formula (2) at $T = 0.085$ K.

field B_\parallel leads to dephasing of Andreev pairs in the normal-metal electrode under the following condition [23]:

$$\frac{\Phi_0}{l_\varphi d_n} \approx 300 - 400 \text{ G.}$$

This estimate is rather close to values in Fig. 8. In view of the qualitative character of estimation, the agreement seems to be quite satisfactory.

Another possible mechanism of suppression of the Andreev conductance was considered in [24]. According to this, the field affects the subgap conductance via spin splitting of electron energy in the pair. However, this effect can only be manifested in fields two to three orders of magnitude greater. Magnetic fields of about 100 G cannot significantly influence the electron energy, since an energy increment equivalent to 0.01 K is much less than the temperature ($0.01 \text{ K} \ll T$).

Judging from the results of our experiments with normal field B_\perp , the estimate of $\Phi_0/l_\varphi^2 \approx 10$ G is more likely to be applicable. However, the situation in this case is rather complex, since the aluminum film rep-

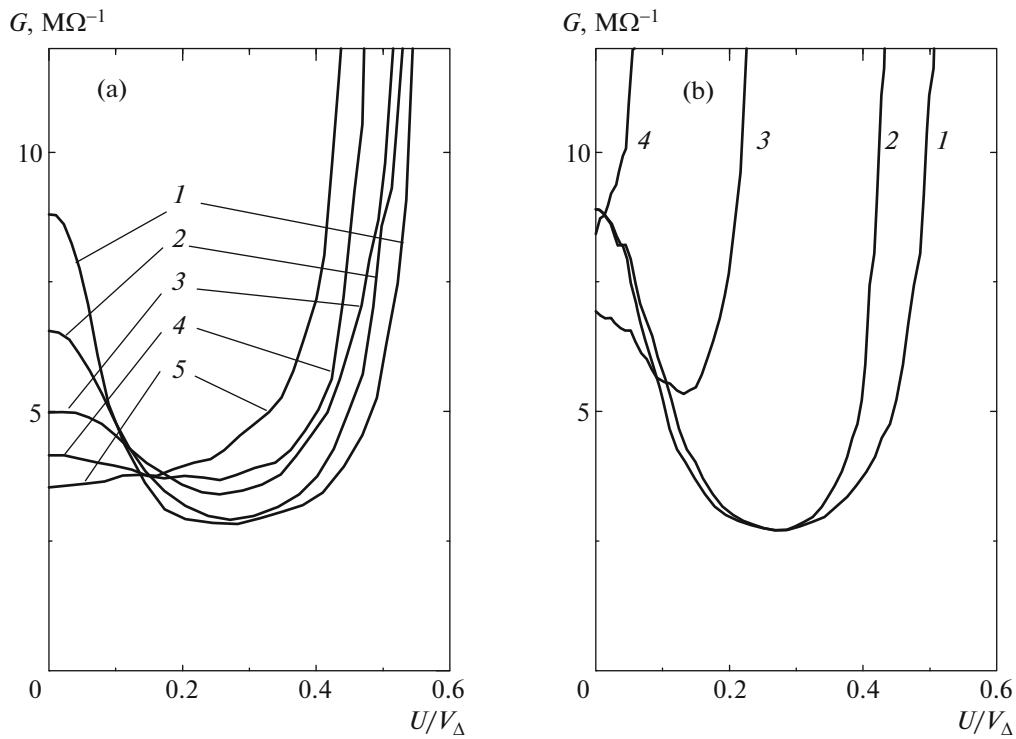


Fig. 6. Plots of conductance G of SIN junction vs. reduced voltage in magnetic field (a) B_{\parallel} at $T = 0.09$ K, H [G] = 0 (1), 95 (2), 140 (3), 180 (4), 235 (5) and (b) B_{\perp} at $T = 0.08$ K, H [G] = 0 (1), 19 (2), 29 (3), 34 (4).

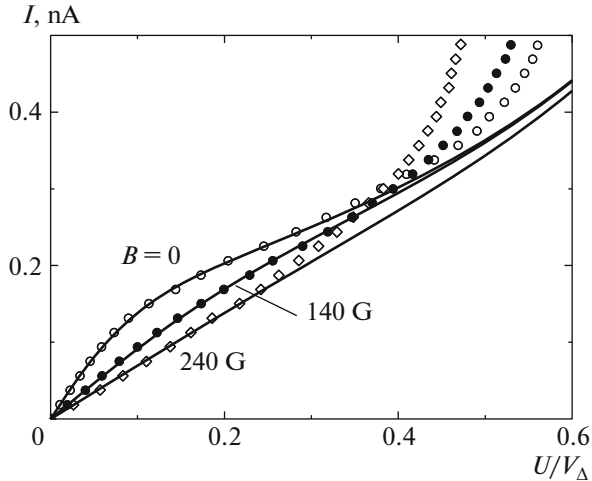


Fig. 7. Plots of the tunneling current of SIN junction vs. reduced voltage at indicated in-plane magnetic fields. Circles show measured $I-U$ characteristics; curves represent calculations by formula (3). Established parameters: $K_n = 0.135$ nA; $K_s = 0.32$ nA; $T_{\text{eff}} = 0.107$ K ($B = 0$), 0.24 K (140 G), and 0.39 K (240 G); $T = 0.09$ K.

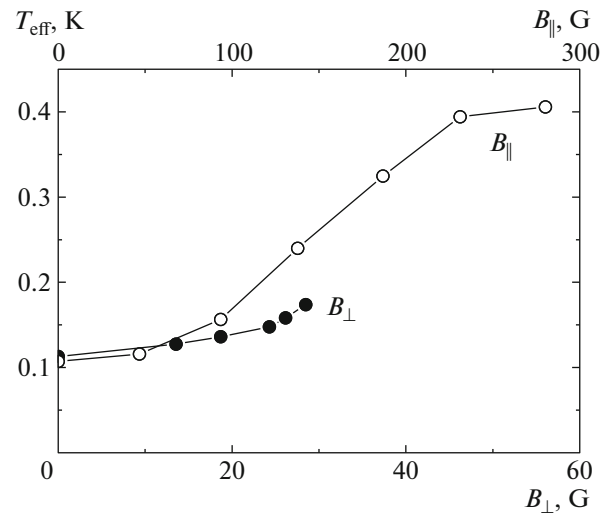


Fig. 8. Plots of $T_{\text{eff}}(B)$ for SIN junction in magnetic field applied along the normal (B_{\perp}) and in the plane (B_{\parallel}) of the junction.

resents a type II superconductor [14]. In fields below the lower critical value, closed currents are excited that produce partial screening of the field. Owing to a rather large penetration depth, $\lambda > 300$ nm, the field penetrates into the volume of superconductor at least

near the junction edges. For $B_{\perp} < 35-40$ G, the state of the junction (as estimated from $I-U$ curves of the type presented in Figs. 6 and 7) exhibits reversible variations depending on the field. At $B_{\perp} > 40-45$ G, the junction jumps into a different state characterized

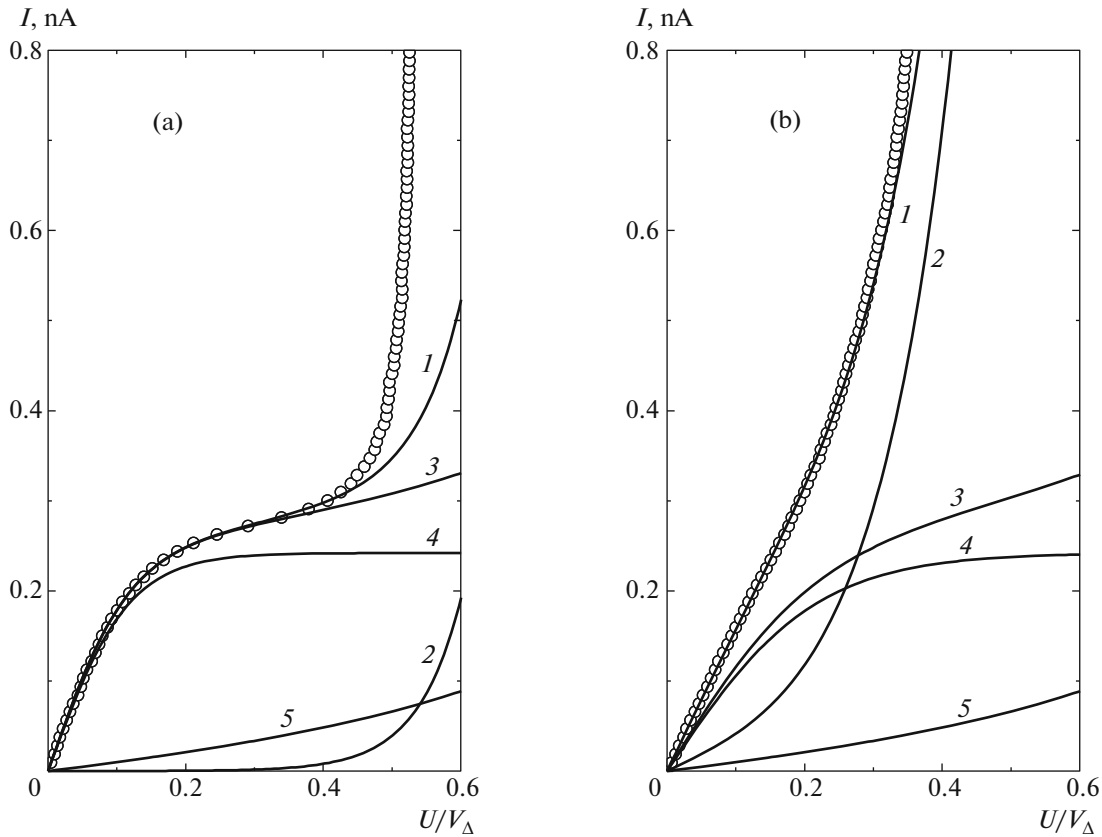


Fig. 9. I – U characteristics (circles) of the SINIS junction aluminum–aluminum oxide–hafnium at the sample holder temperature of (a) 0.085 K and (b) 0.215 K: (1) calculated total current; (2) single-particle current calculated by formula (2) for $T = 0.12$ K (a) and 0.215 K (b), $\Delta_c = 1.9$ K, and $R_n = 480 \Omega$; (3) total Andreev current including I_n (4) and I_s (5) calculated by formula (3) with $K_n = 0.24$ nA, $K_s = 0.09$ nA, $T_{\text{eff}} = 0.11$ (a) and 0.205 K (b).

by a tenfold change in the conductance at $U = 0$. This state probably corresponds to the penetration of Abrikosov vortices into the volume of superconductor. The corresponding pattern of vortices was observed by the decoration technique on mesoscopic niobium films [25], where the presence of a barrier for vortex penetration was established. The pinning of vortices led to hysteresis, since the field switch-off was insufficient for the return to a state with low conductance and it was necessary to switch on the field of opposite polarity or heat the sample in zero field to a temperature above T_c . Naturally, this behavior of the superconducting film in the magnetic field complicates the interpretation of experimental data not only for the Andreev current but also for the single-particle tunneling current, the more so that the mechanism of field influence in the latter case is still unknown.

According to the model [12], current I_s is related to the motion of pairs in the superconductor. The correlation length ξ in the aluminum film does not exceed $0.1 \mu\text{m}$ [14]. Accordingly, the estimation of a field sufficient for suppressing this current yields $B_{\parallel} \approx 2500$ G

and $B_{\perp} \approx 1000$ G, which is an order of magnitude greater than the fields used in the present work.

A decrease in the Andreev conductance can be partly explained by decreasing area of the superconducting layer, which is caused by the penetration of quantum vortices into this layer. However, taking into account the results obtained in [14] for $B_{\perp} \approx 20$ – 30 G, we conclude that the cores of Abrikosov vortices occupy no more than 5% of the junction area and, hence, these vortices cannot significantly influence the subgap two-particle current.

3. INVESTIGATION OF ALUMINUM–ALUMINUM OXIDE–HAFNIUM STRUCTURES

Aluminum–aluminum oxide–hafnium tunnel structures were manufactured by the same technology [15] as that used for the above-described samples with copper electrodes and also comprised several structures on a common silicon substrate. It turned out that the yield of structures suitable for measurements was not high: only one SINIS structure with a junction

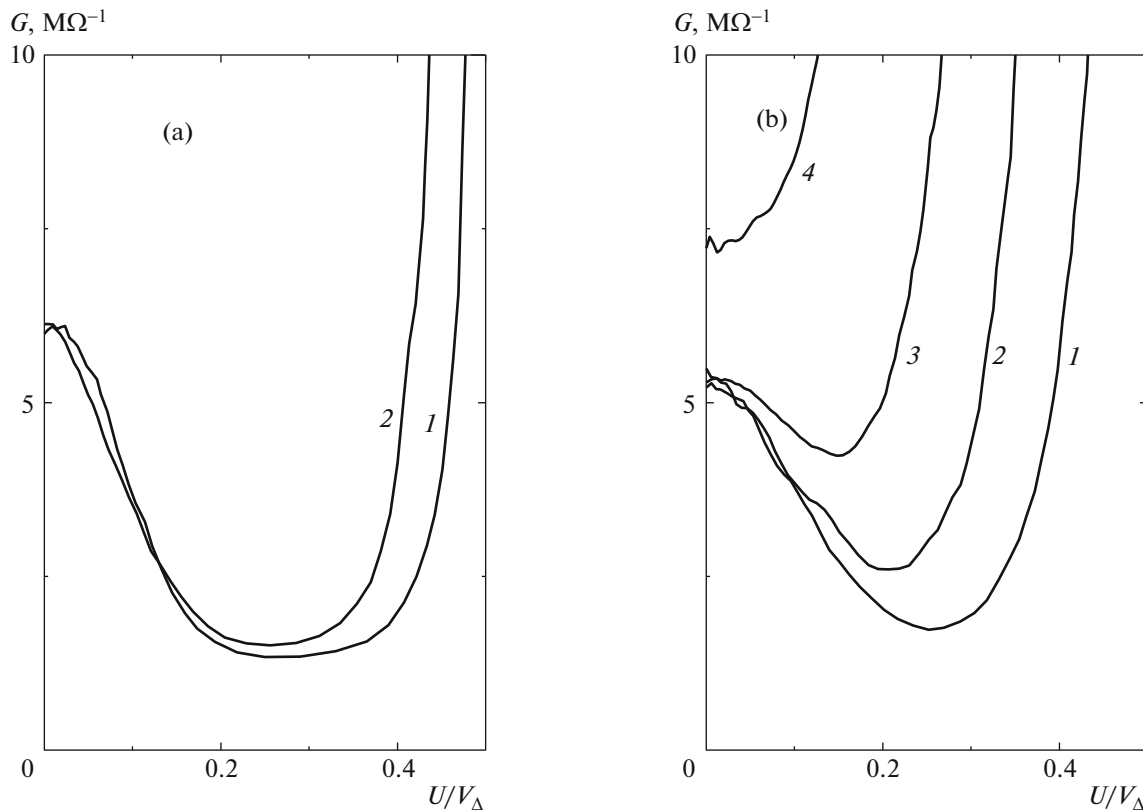


Fig. 10. Plots of conductance G of SINIS junction aluminum–aluminum oxide–hafnium vs. reduced voltage in magnetic field applied (a, experiment of December 21, 2015) in plane of the junction at $T = 0.09$ K, H [G] = 0 (1), 285 (2) and (b, experiment of March 15, 2016) perpendicular to the junction at $T = 0.11$ K, H [G] = 0 (1), 35 (2), 47 (3), 60 (4).

area of $8 \mu\text{m}^2$ exhibited a clearly pronounced subgap conductance and 1000-fold drop in the single-particle conductance upon cooling below 0.1 K (Figs. 9 and 10).

The values of parameters Δ_c and R_n for these structures (as well as for those with copper electrodes) were determined from the temperature dependence of conductance $G(U=0, T)$. However, the error of Δ_c and R_n measurements in these samples was several times larger. This circumstance was caused by the fact that the resistance of current-carrying paths connecting contact pads to the SINIS structure was rather large (about $5 \text{ k}\Omega$), markedly exceeded the R_n value (300–500 Ω per junction), and was comparable with differential resistance R_d at temperatures within 0.4–0.5 K. The Δ_c values fell within 1.7–1.9 K. In the temperature interval of 0.25–0.5 K, the best fit of calculated $G(U)$ curve to experimental data was achieved with $\Delta_c = 1.7$ K, but the calculated temperatures below 0.2 K turned out to be 0.1–0.2 K lower than the temperature of sample holder. In this region, a more realistic temperature estimate was assumed to be $\Delta_c = 1.9$ K. In addition, junctions to hafnium exhibited a significant overheating by the probing current, as is clearly

revealed by comparison of Figs. 3a and 9a. This behavior correlates with a large resistance of connecting paths deteriorating heat removal from the structure. In the structure with hafnium, experimental points for increasing voltage on the junction more significantly deviate from the calculated curve than in the case of copper bridges. It should also be noted that overheating is already observed at zero current: experimental I – U curves measured at sample holder temperatures of 0.085 and 0.11 K in the region of single-particle conductance coincide to within the accuracy of measurements. This is probably related to the action of parasitic electromagnetic signals.

It is commonly accepted that hafnium is a superconductor. However, the available published data on its superconductivity and critical temperature are rather contradictory, including the absence of superconductivity at $T > 0.015$ K [26], appearance of superconductivity at $T < 0.374$ K upon long-term annealing [27] (close to the value reported earlier [28]), and superconductivity with $T_c = 0.128$ K [29]. To the best of our knowledge, no data on the superconductivity of hafnium films have been reported so far.

In the structures under consideration, no qualitative changes indicative of the appearance of superconductivity in hafnium films were observed. Indeed, if the SIN junction were converted into SIS junction, then the Josephson current would be observed at $U = 0$ and the measured voltage would be determined by the resistance of the connecting paths, which was about 5 k Ω . In our experiments, it was much greater and amounted to $R_d(U = 0) \approx 200$ k Ω . Hysteretic phenomena were also not observed. For the SIS junction, the first zero of Josephson current in the structure with lateral dimensions about 1 μm and the total thickness of about 80 nm (the penetration depth in “impure” films studied exceeded their thicknesses) must be observed in a tangent field of about 250 G. It has been established (see below) that the conductance at $U = 0$ in these fields exhibits no changes at all. Therefore, the superconductivity of hafnium films, as a factor determining the observed peculiarities of $I-U$ curves, can be excluded in the entire range of temperatures $T > 0.1$ K.

Qualitatively, the $I-U$ curves of the structures with hafnium measured in the region of subgap conductance were similar to the curves of structures with copper. Proceeding from this, we described these curves using the above approach based on relation (3) and determined the same parameters K_n , K_s , and T_{eff} as those for the samples with copper bridges. Among these quantities, only T_{eff} depended on the temperature and was $T_{\text{eff}} \approx T$ (see Fig. 4). The values of the parameters are presented in the table (lines 16 and 17). It was found that K_n and K_s varied from one experimental run to another and had the same order of magnitude as the values for structures with copper bridges, although the ratios of normal resistances for the Andreev mechanism according to formula (1) allowed a decrease by two orders of magnitude to be expected for hafnium. The value of K_n calculated according to formula (1) for the density of states of $2.6 \times 10^{47} \text{ J}^{-1} \text{ m}^{-3}$ in hafnium [19] is given in the table and is also two orders of magnitude lower than the measured value. This is probably explained by inhomogeneity of the insulating layer, such that the area of a transparent tunnel contact amounts to a small fraction (on the order of or below 0.1) of its geometric area. For the same reason, R_n is also about one order of magnitude greater than the value for junctions with copper.

The results of measurements in magnetic fields showed that variations of the single-particle conductance (Fig. 10) observed in the structures with hafnium are generally analogous to those in samples with copper bridges (Fig. 6). However, the subgap Andreev conductance is independent of the field (Fig. 10), which is probably due to the diffusion length with phase loss being much lower in hafnium than in copper.

It can be suggested that the observed difference of SIN structures with hafnium from those with copper is related to differences in the mechanism of subgap conductance, for example, the presence of fluctuating pairs in hafnium. As is known, fluctuations decrease the tunnel conductance at $T > T_c$ because of a decrease in the density of states near the Fermi level, but they can increase the tunnel conductance [30]. Unfortunately, situations close to our experiments were not analyzed in [30].

4. INVESTIGATION OF ALUMINUM–ALUMINUM OXIDE–ALUMINUM WITH IRON SUBLAYER STRUCTURES

In this part, we studied structures on silicon comprising a 0.8-nm-thick Fe sublayer suppressing superconductivity in the subsequently deposited 12-nm-thick Al layer, 1-nm-thick gate layer of aluminum oxide, and 80-nm-thick superconducting Al layer. This sample was previously studied in [14].

The measurements were performed on a chain of 100 serially connected SIN junctions with dimensions of $2 \times 1 \mu\text{m}^2$. The gap Δ_c was determined using $G(T)$ curves and R_n values measured for the chain of electrodes with connecting paths. The agreement of measured and calculated $G(T)$ values showed that the contribution of normal metal regions to the resistance of serially connected junctions was negligibly small. The values of Δ_c and R_n are presented in the table (line 18). The subgap conductance in this structure is not as clearly pronounced as in samples described above (Fig. 11), but a significant difference from the single-particle tunneling is evident. Taking into account the large dynamic resistance (on the order of 100 M Ω) at zero voltage, it can be suggested that the observed pattern is due to shunting of the single-particle conductance by the input resistance of amplifier, hardly controllable leaks between contacts at room temperature, and microscopic “pinholes” in the tunnel barrier. However, the shunting by voltage-independent resistance would lead to a pattern that must be qualitatively different (Fig. 11b, curve 3) from the observed one.

The conductance per single SIN junction amounts to 1.2 M Ω^{-1} and is comparable (the more so, taking into account the smaller junction area) to the Andreev conductance of structures with copper bridges. Proceeding from this, we again described the experimental data using the above approach based on relation (3). A qualitative difference from the cases considered above consists in the absence of a maximum on the $G(U)$ dependence at $U = 0$. As can be seen from Fig. 12, this dependence is nonanalytic, which is characteristic of the I_s component according to formula (3). However, with neglect of the I_n contribution, the $G(U)$ dependence cannot be described in the region of U/V_Δ from 0 to 0.5 with accuracy better than 10–20%. A good agreement of the calculations by formula (3) and

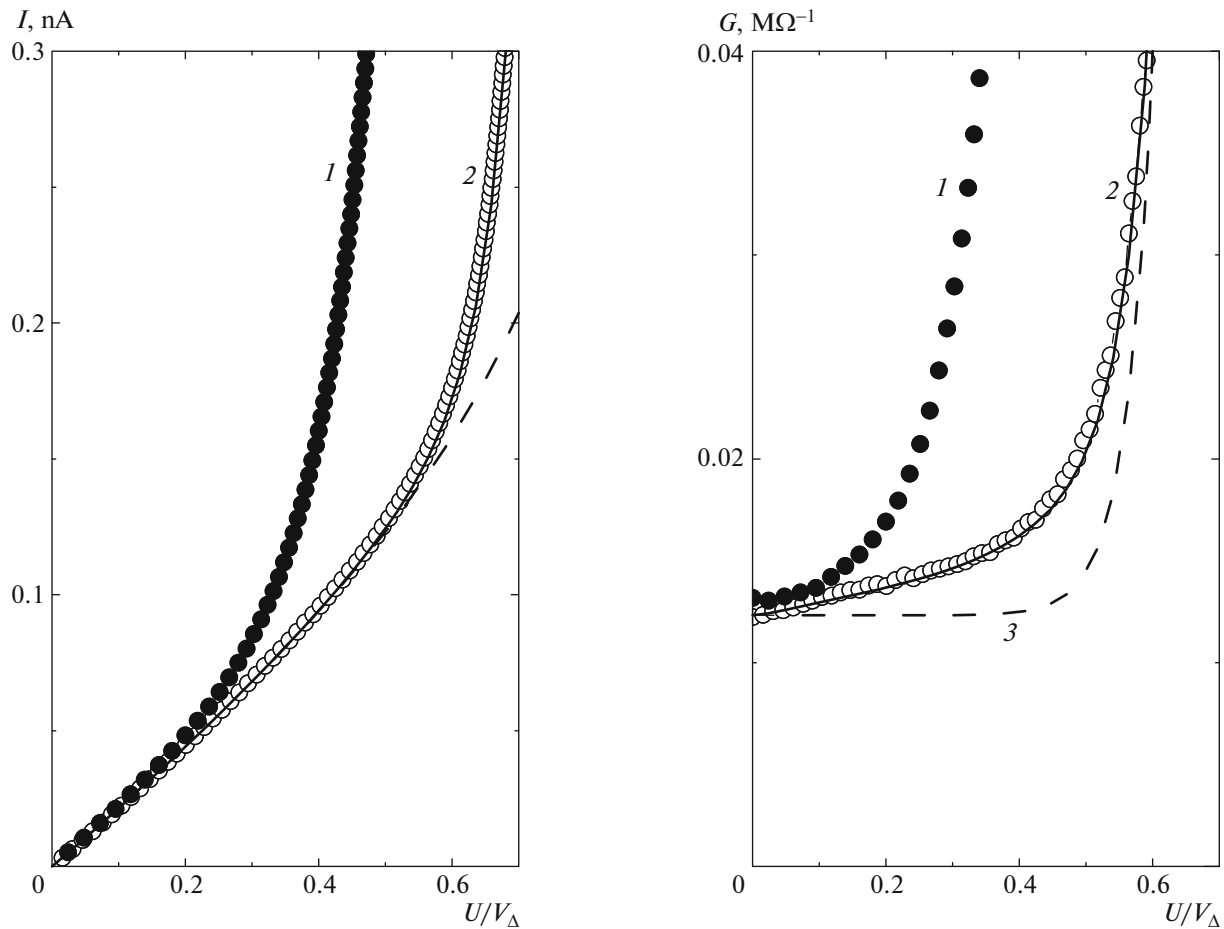


Fig. 11. (a) $I-U$ characteristics and (b) dynamic conductance of multielement SIN junction aluminum–aluminum oxide–aluminum with Fe sublayer. Points show results of measurements at $T = 0.13$ K (1) and $T = 0.08$ K (2). Dashed line in (a) represents calculation of the Andreev current; solid curves show the calculations of (a) total current and (b) conductance; dashed curve 3 shows the conductance at $T = 0.08$ K calculated under assumption of the absence of Andreev conductance and for the shunting of junction by 80 M Ω resistor.

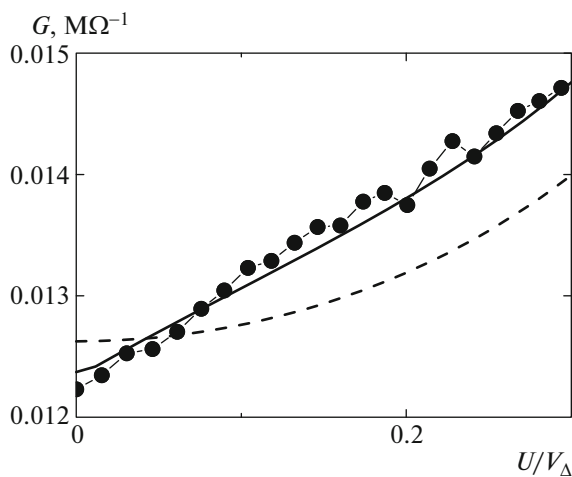


Fig. 12. Initial part of the experimental $G(U)$ dependence at $T = 0.08$ K (points) in comparison to approximations by formula (3) (solid line) and formula (4) (dashed curve).

experiment is reached with parameters presented in the table (line 18). As can be seen from these data, K_n and K_s (with allowance for the smaller junction area) fall in the same range as those for other junctions. However, the value of $T_{\text{eff}} = 0.56$ K turns out to be anomalously high and significantly exceeds the sample temperature. This situation agrees with the fact that $G(0)$ is virtually independent of the temperature (see Fig. 11b). For the measurements in magnetic fields $B_{\perp} \leq 30-40$ G, the conductance at zero bias voltage also remained unchanged [14].

Figure 12 shows the initial part of the $G(eU/V_{\Delta})$ dependence. As can be seen, the conductance is a linear function of the voltage. This behavior could be observed because component G_n was relatively small and the noises accompanying voltage measurements were also relatively small owing to summation of the voltage on 100 serially connected junctions. A comparison of the functions described by formulas (3) and

(4) qualitatively demonstrates the inapplicability of a popular approach based on the idea that the spectrum of quasi-particles with energies close to the gap width exhibits broadening due to their finite decay. However, the problem of significant quantitative discrepancies between I_s values calculated by formula (1) and those determined by fitting formula (3) to experiment does not allow the model proposed in [12] to be unconditionally accepted.

As is known, iron dissolves in aluminum at elevated temperatures [31]. Naturally, this process significantly slows down at room temperature, but nevertheless takes place for periods of time within several dozen or several hundred days. Iron atoms (possessing magnetic moment) present in the aluminum matrix accelerate the dephasing of electrons during their diffusion and suppress (by analogy with the external magnetic field) the subgap conductance in tunnel structures.

5. CONCLUSIONS

The results of our experiments showed that the anomalies observed at low bias voltages in the $I-U$ curves of various SIN structures are caused by two-particle tunneling with the Andreev reflection of electrons at the superconductor–normal metal boundary with insulating barrier layer. The current in this region can be subdivided into two components: I_n , dependent on the temperature and magnetic field, and I_s , independent of these variables. The latter component has frequently been described in the framework of the Dynes model, but our results show that the use of this theory is incorrect. The experiment is well described by the functional dependence $I(U, T)$ according to relation (3) that follows from theory [12]. However, if the experimental values of current I_n differ from theoretical predictions not very significantly, the theoretical value of I_s is several dozen times lower than the measured value. A not less significant fact is that the K_s/K_n ratio (which must be proportional for the given pair of metals to only the ratio of thicknesses of the normal and superconducting layers and be constant for structures manufactured in one technological cycle) varies in rather broad limits of 2–7 (see table, lines 1–13). Therefore, it may be concluded that the theory takes into account not all important factors and the knowledge of area-averaged characteristics of tunnel structures is insufficient for adequate description of their subgap conductance.

It was established that the properties of SIN microstructures exhibit significant temporal variation. This is apparently a natural process related to the corrosion and mutual diffusion of structural materials. In order to elucidate this issue, it is necessary to study the composition, structure, and dynamics of interfaces, which is hardly possible without destruction of a sample.

The magnetic field, irrespective of its orientation, influences the Andreev and single-particle conductances with opposite trends, suppressing the former and sharply increasing the latter. The field effect on the Andreev conductance can be understood on the basis of phase variation in the superconducting electrode. As for the single-particle conductance, an evident assumption that normal regions with high conductivity appear in the superconductor, as was demonstrated in [14], is by no means sufficient for explaining the shapes of observed $I-U$ curves. This issue also requires additional investigation.

ACKNOWLEDGMENTS

We are grateful to A.F. Andreev for his interest in this work; to A.F. Volkov, Yu.V. Nazarov, A.G. Semenov, A.D. Zaikin, and I.N. Khlyustikov for fruitful discussions; and to A.O. Fedotov and S.A. Lemzyakov for their assistance. This work was supported in part by the Ministry of Education and Science of the Russian Federation (project no. 14.607.21.0100; identifier code RFME-FI60714X0100).

REFERENCES

1. F. Giazotto, T. T. Heikkil, A. Luukanen, et al., *Rev. Mod. Phys.* **78**, 217 (2006).
2. A. V. Feshchenko, L. Casparis, I. M. Khaymovich, et al., *Phys. Rev. Appl.* **4**, 034001 (2015).
3. H. Q. Nguyen, M. Meschke, H. Courtois, and J. P. Pekola, *Phys. Rev. Appl.* **2**, 054001 (2014).
4. M. Tarasov, V. Edelman, A. Ermakov, et al., *IEEE Trans. Terahertz Sci. Technol.* **5**, 44 (2015).
5. G. E. Blonder, M. Tinkham, and T. M. Klapwijk, *Phys. Rev. B* **25**, 4515 (1982).
6. H. Pothier, S. Gueron, D. Esteve, and M. H. Devoret, *Phys. Rev. Lett.* **73**, 2488 (1994).
7. S. Rajauria, P. Gandit, T. Fournier, et al., *Phys. Rev. Lett.* **100**, 207002 (2008).
8. H. Courtois, S. Rajauria, P. Gandit, et al., *J. Low. Temp. Phys.* **153**, 325 (2008).
9. P. J. Lowell, G. C. O'Neil, J. M. Underwood, and J. N. Ullom, *J. Low. Temp. Phys.* **167**, 392 (2012).
10. T. Greibe, M. P. V. Stenberg, C. M. Wilson, et al., *Phys. Rev. Lett.* **106**, 097001 (2011).
11. A. V. Seliverstov, M. A. Tarasov, and V. S. Edel'man, *JETP Lett.* **103**, 484 (2016).
12. F. W. J. Hekking and Yu. V. Nazarov, *Phys. Rev. B* **49**, 6847 (1994).
13. A. G. Semenov, A. D. Zaikin, and L. S. Kuzmin, *Phys. Rev. B* **86**, 144529 (2012).
14. M. A. Tarasov and V. S. Edel'man, *JETP Lett.* **101**, 740 (2015).
15. M. A. Tarasov, V. S. Edel'man, M. Yu. Fominskii, et al., *Zh. Radioelektron.*, No. 1 (2016).
16. V. S. Edelman, *Instrum. Exp. Tech.* **52**, 301 (2009).

17. D. Golubev and L. Kuzmin, *J. Appl. Phys.* **89**, 6464 (2001).
18. B. Pannetier, J. Chaussy, and R. Rammal, *Phys. Scripta T* **13**, 245 (1986).
19. G. D. Kneip, Jr., J. O. Betterton, Jr., and J. O. Scarborough, *Phys. Rev.* **130**, 1687 (1963).
20. N. E. Phillips, *Phys. Rev.* **114**, 676 (1959).
21. A. F. Volkov and T. M. Klapwijk, *Phys. Lett. A* **168**, 217 (1992).
22. A. F. Volkov, *JETP Lett.* **55**, 746 (1992).
23. D. A. Dikin, M. J. Black, and V. Chandrasekhar, *Phys. Rev. Lett.* **87**, 187003 (2001).
24. A. G. Semenov and A. D. Zaikin, arXiv:1410.7932.
25. I. V. Grigorieva, W. Escoffier, J. Richardson, et al., *Phys. Rev. Lett.* **96**, 077005 (2006).
26. J. E. Cox, *Phys. Lett. A* **28**, 326 (1968).
27. T. S. Smith and J. G. Dfunt, *Phys. Rev.* **88**, 1172 (1952).
28. N. Kurti and F. Simon, *Proc. R. Soc. London A* **151**, 610 (1935).
29. B. W. Roberts, *J. Phys. Chem. Ref. Data* **5**, 581 (1976).
30. A. Glatz, A. A. Varlamov, and V. M. Vinokur, arXiv:1210.4206.
31. O. A. Bannykh, P. B. Budberg, S. P. Alisova, et al., *State Diagrams of Binary and Multicomponent Systems Based on Iron* (Metallurgiya, Moscow, 1986) [in Russian].

Translated by P. Pozdeev